The POWER Experiment: Impact of Assimilation of a Network of Coastal Wind Profiling Radars on Simulating Offshore Winds in and above the Wind Turbine Layer

Irina V. Djalalova,[a,b] Joseph Olson,[a,b] Jacob R. Carley,[c] Laura Bianco,[a,b]
James M. Wilczak,[b] Yelena Pichugina,[a,b] Robert Banta,[b]
and Melinda Marquis,[b] and Joel Cline[d]

[a] *University of Colorado/Cooperative Institute for Research in Environmental Sciences, Boulder, Colorado*
[b] *NOAA/Earth Systems Research Laboratory, Boulder, Colorado*
[c] *I. M. Systems Group, Inc., and NOAA/NWS/Environmental Modeling Center, College Park, Maryland*
[d] *Office of Energy Efficiency and Renewable Energy, Department of Energy, Washington, D.C.*

ABSTRACT

During the summer of 2004 a network of 11 wind profiling radars (WPRs) was deployed in New England as part of the New England Air Quality Study (NEAQS). Observations from this dataset are used to determine their impact on numerical weather prediction (NWP) model skill at simulating coastal and offshore winds through data-denial experiments. This study is a part of the Position of Offshore Wind Energy Resources (POWER) experiment, a Department of Energy (DOE) sponsored project that uses National Oceanic and Atmospheric Administration (NOAA) models for two 1-week periods to measure the impact of the assimilation of observations from 11 inland WPRs. Model simulations with and without assimilation of the WPR data are compared at the locations of the inland WPRs, as well as against observations from an additional WPR and a high-resolution Doppler lidar (HRDL) located on board the Research Vessel *Ronald H. Brown* (*RHB*), which cruised the Gulf of Maine during the NEAQS experiment. Model evaluation in the lowest 2 km above the ground shows a positive impact of the WPR data assimilation from the initialization time through the next five to six forecast hours at the WPR locations for 12 of 15 days analyzed, when offshore winds prevailed. A smaller positive impact at the *RHB* ship track was also confirmed. For the remaining three days, during which time there was a cyclone event with strong onshore wind flow, the assimilation of additional observations had a negative impact on model skill. Explanations for the negative impact are offered.

1. Introduction

Because of their smaller greenhouse gas emission footprint, renewable energy sources, such as wind, solar, tidal, and geothermal have been looked at with particular interest in past decades. These energy sources, although clean and abundant in nature, have the limitation of being variable over time, making the accuracy of numerical weather prediction (NWP) models critical to their use. Among the above-mentioned renewable sources, offshore wind energy is particularly appealing because of its potential to supply coastal energy loads, which have limited access to long-distance interstate grid transmission.

Previous studies have provided model-based maps of U.S. offshore wind energy resources out to a distance of 50 n mi (1 n mi = 1.852 km) with detailed analyses of water depth and distance from the shore (e.g., Schwartz et al. 2010; Musial and Ram 2010). These studies demonstrate that the East Coast, and especially the northern East Coast, has excellent potential as a wind resource with extensive regions of shallow water relatively far from shore, which makes offshore wind power plants less costly to build and maintain. Typical annual-averaged wind speeds in the northern East Coast

Corresponding author address: Irina V. Djalalova, NOAA/Earth System Research Laboratory, 325 Broadway, MS PSD3, Boulder, CO 80305.
E-mail: irina.v.djalalova@noaa.gov

region are higher than $7\,\mathrm{m\,s^{-1}}$ near turbine hub heights (approximately 90 m above the surface of the ocean). Despite the potential for offshore wind energy development, there is a lack of reliable wind observations at the heights of turbine rotors over the ocean, generally as a result of the high cost of offshore measurements. For this reason, we used data from a field campaign, the New England Air Quality Study (NEAQS), which took place during the summer of 2004 and was conducted to study air quality off the New England coast in the Gulf of Maine, as a source of data for studying the skill of NWP models in simulating coastal and offshore winds. As this is a region slated for potential offshore wind energy development, we took advantage of the availability of this unique dataset to measure the impact of assimilating additional observations on the model performance, using onshore and offshore data for verification of model skill.

During the NEAQS campaign, 11 onshore coastal and inland sites were equipped with wind profiling radars (WPRs), while the NOAA Research Vessel *Ronald H. Brown* (hereafter called *RHB*) was used as a movable offshore platform equipped with several other measuring systems (Angevine et al. 2006). Observations from the 11 WPRs were used in this study for assimilation in NWP models and also for verification, while the instruments located on the *RHB* [particularly one WPR and one high-resolution Doppler lidar (HRDL)] were used for evaluation purposes only.

This manuscript is organized as follows. Section 2 introduces the dataset collected during the NEAQS 2004 campaign. Section 3 describes the four NWP models used in this study, as well as the data assimilation methodology, and shows the model performance in the lower boundary layer of the study area. Section 4 evaluates the impact of the assimilation of the extra 11 WPRs at the inland WPR sites. Section 5 analyzes the
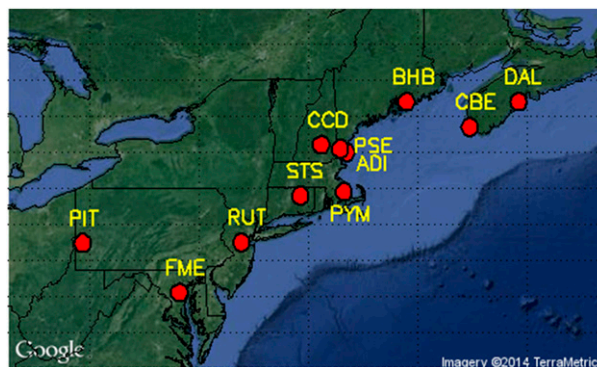

FIG. 1. Location of the inland WPRs in New England and Nova Scotia.

impact from assimilating the 11 WPRs at the *RHB* locations. Conclusions are discussed in section 6.

2. The dataset: NEAQS 2004 measurement campaign

a. Inland wind-profiling radars

The instrument dataset involved in the Position of Offshore Wind Energy Resources (POWER; Banta et al. 2014) project included a network of 11 inland WPRs (Strauch et al. 1984; Wilczak et al. 1996; McKeen et al. 2007) used for NEAQS during the summer of 2004 (Fig. 1). They were mostly located along the New England and Nova Scotia coastline.

Wind profiling radars are Doppler radars that do not require a hard target to receive a backscattered signal. In the clear-air atmosphere, WPRs receive backscattered signals from refractive index inhomogeneities (Carter et al. 1995). All WPRs used during NEAQS-2004 were 915-MHz radars (33-cm wavelength), with the lowest range gate centered at around 120 m above ground level (AGL). Two sampling modes were used by the

TABLE 1. Operational specification for the wind profiling radars deployed during NEAQS-2004.

Site	Location	High-resolution specifications			Low-resolution specifications		
		First height (m)	Gate spacing (m)	No. of gates	First height (m)	Gate spacing (m)	No. of gates
ADI	Appledore, ME	123	58	38	109	101	38
BHB	Bar Harbor, ME	123	58	38	130	100	38
CBE	Chebogue Pt., NS	123	58	38	130	102	38
CCD	Concord, NH	122	58	38	129	102	38
FME	Ft. Mead, MD	124	55	36	282	96	40
PYM	Plymouth, MA	138	58	38	129	102	38
PIT	Pittsburgh, PA	114	58	45	39	96	58
PSE	Pease Tradeport, NH	85	60	72	—	—	—
RHB	*Ronald H. Brown*	216	58	52	310	101	55
RUT	New Brunswick, NJ	124	55	36	158	96	59
STS	Storrs, CT	71	52	95	272	110	71
DAL	Lunenburg, NS	199	96	33	275	192	30

instruments: a high-resolution mode with a vertical gate spacing of about 60 m and a low-resolution mode with a vertical gate spacing of about 100 m. The maximum height with detectable signal varies with atmospheric conditions (e.g., a stronger signal occurs in a moister atmosphere), but the coverage typically ranges from the lowest level up to around 1.5 km AGL for the high-resolution mode and up to around 4 km AGL for the low-resolution mode. One radar in this study [at Portsmouth International Airport at Pease, Portsmouth, New Hampshire (PSE)] only used a high-resolution mode. The different operational specifications used for the various NEAQS-2004 WPRs are summarized in Table 1. All WPR data were reprocessed using a modified Weber–Wuertz quality control module (Weber et al. 1993) to compute the hourly winds. The modified version performs time–height continuity checks on the moment-level radial velocities, derives meteorological-component velocities using the continuity-controlled radial velocities, and then applies final time–height continuity checks on the U, V, and W wind components.

b. Offshore instruments (WPR and HRDL)

The major offshore measurement platform was the *RHB*, which cruised around the Gulf of Maine recording meteorological, air chemistry, and some oceanographic data from 9 July to 12 August 2004. Instrumentation important to the present study located on the ship included NOAA's HRDL and a 915-MHz WPR. Both instruments were permanently deployed on the ship and their measurements were corrected in real time for ship motion including pitch and roll. The sampling mode specifications for the WPR on the *RHB* are included in Table 1. The data collected during 2004 by the *RHB* WPR have been reprocessed for the POWER experiment, using up-to-date postprocessing wind profiler algorithms in order to reduce contamination from sea clutter.

The HRDL is a scanning Doppler lidar similar in concept to a Doppler weather radar, although the scattering targets are aerosol particles rather than hydrometeors. This makes the Doppler lidar useful for mapping the wind field in clear air since aerosol particles are widely distributed in the atmospheric boundary layer and especially near the surface of the ocean, where sea salt particles are effective backscatter targets. Technical characteristics of the lidar system used in this study are given in Table 2 (Grund et al. 2001; Pichugina et al. 2012).

The WPR and HRDL have their relative strengths and limitations. The WPR has a 60–100-m range gate spacing with a first range gate typically near 120 m above sea level (ASL). Its measurements can be degraded by sea clutter contamination in the lowest ~500 m of the

TABLE 2. Technical characteristics of NOAA/ESRL Doppler lidar.

HRDL parameter	Value
Wavelength	2.02 μm
Pulse energy	2.0 mJ
Pulse rate	200 Hz
Gate range	30 m
Velocity precision	~10 cm s^{-1}
Time resolution	0.5 s
Min range	189 m
Max range (horizontal)	3–8 km

atmosphere when measuring over the ocean, which requires careful quality control of the data.

In contrast, HRDL's azimuth and elevation scanning capability allow frequent, high-vertical-resolution profiling of the winds. The HRDL has a 30-m range resolution with a first range gate at 189 m. From the conical scanning schemes, wind profiles are averaged at vertical intervals of less than 10 m and over time intervals of several minutes, starting within a few meters of the ocean surface. For this reason, the strength of the HRDL is in monitoring low-level winds, below the minimum range gate of the WPR. HRDL does not collect useful measurements during fog or in clouds. On the other hand, the WPR measurements extend to a greater height than that reached by HRDL and provide useful data in cloud and fog conditions. For this reason we used these two instruments complementarily.

During the NEAQS experiment GPS rawinsondes were launched from the *RHB* from four to six times per day. Comparisons of the rawinsondes, lidar, and WPRs showed very good agreement (Wolfe et al. 2007) validating the overall quality of the deployed instrumentation. The correlation between rawinsondes and WPR is in the range 0.88–0.94 up to 2 km above the ocean, and the correlation between rawinsondes and HRDL is equal to 0.97 in a 1-km slice above the ocean.

The criterion for selecting the time periods analyzed in the current study is based primarily on the availability of several consecutive days of HRDL measurements in order to provide a continuous dataset to compare modeled verus measured winds in the turbine-rotor layer over the ocean. The first study period selected was 6–12 August, corresponding to the longest lull between frontal passages according to White et al. (2007). For the second study period (10–17 July), two shorter periods separated by a day of rain were chosen, so that model runs could be performed continuously for a week without having to restart. Although the intervening rainy period was not originally contemplated for the analysis, we later decided to include it as it turned out to be quite interesting for the model evaluation.
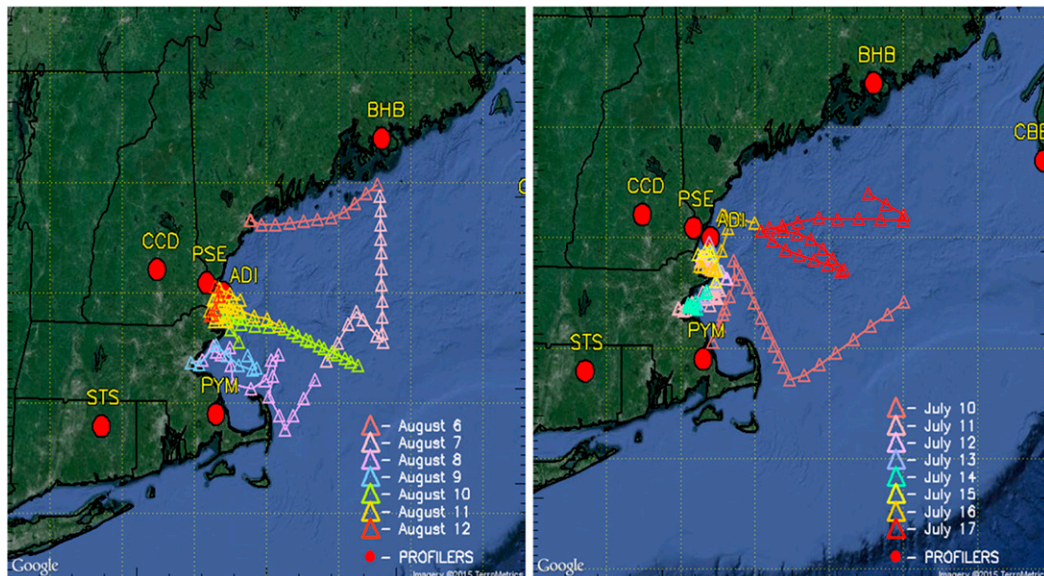
FIG. 2. *RHB* daily ship track for the chosen time periods: (left) 6–12 Aug and (right) 10–17 Jul 2004.

The locations of the *RHB* during the two selected periods are shown in Fig. 2 along with the locations of nearby WPRs. On most days the ship was in coastal waters close to shore, but on 6 days the ship cruised farther out, well into the Gulf of Maine.

3. NWP models

In this study, the observed data collected in 2004 during the NEAQS experiment have been compared to NWP models running at the NOAA/National Weather Service (NWS)/National Centers for Environmental Prediction (NCEP) and NOAA/Earth System Research Laboratory (ESRL)/Global Systems Division (GSD). These are 1) the Rapid Refresh (RAP) model and 2) its associated High-Resolution Rapid Refresh (HRRR) model, both of which are based on the Advanced Research version of the Weather Research and Forecasting (ARW) Model; 3) the hourly updated North American Mesoscale Rapid Refresh Forecast System (NAMRR; Carley et al. 2015) and 4) and its associated, hourly updated, continental United States (CONUS) nest, both of which are based on the Nonhydrostatic Multiscale Model on the B grid (NMMB; Janjić 2003; Janjić 2005; Janjić and Black 2007; Janjić and Gall 2012). The NAMRR is based upon the operational North American Mesoscale Forecast System (NAM), which produces 84-h forecasts every 6 h and features an assimilation cycle only for the 12-km domain. NAMRR was developed as a part of this POWER study to provide cycled, hourly forecasts on both its 12- and 4-km domains. The NAMRR parent domain and the RAP models are run at horizontal grid intervals of 12 and 13 km, respectively. The NAMRR's CONUS nest domain, which is nested within the NAMRR's 12-km grid, features a horizontal grid interval of 4 km. The HRRR, which is run externally from the 13-km RAP (i.e., not nested), features a horizontal grid interval of 3 km (see Fig. 3 for the model domains). A spatially truncated version of the HRRR was used for POWER simulations, centered on the New England region. Both NAMRR and RAP systems used the Climate Forecast System Reanalysis (CFSR; Saha et al. 2010) for lateral boundary conditions.

For the POWER study, these four models were run twice. For the first run, called the control run, the observational data from the network of 11 inland WPRs were not assimilated into the models. For the second run, called the experimental run, these data were assimilated into each run of the hourly updated models. Both the control and experimental simulations assimilated standard observations, including radiosondes, satellite data, and surface observations including buoy measurements.

a. RAP and HRRR

The RAP model serves as NCEP's regional short-range rapidly updating forecast system, providing hourly updated forecasts out to 12 h for the POWER study. It is based on the ARW model (Skamarock et al. 2008). A brief description of the model's parameterization schemes is given in Table 3, and the full description of the RAP version used in POWER can be found online (http://ruc.noaa.gov/pdf/RAPbrief.NCEP-Dir-20Mar2012.pdf).
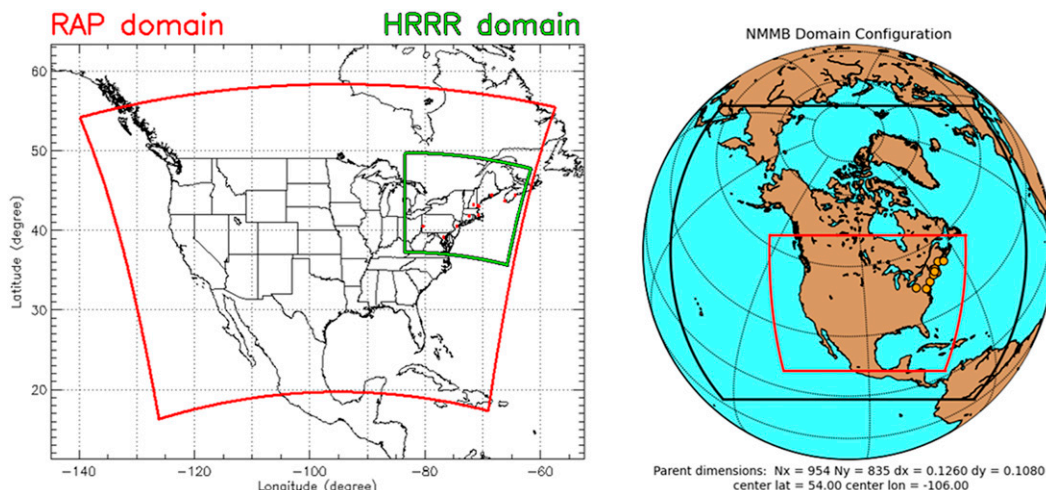
FIG. 3. Domains for NWP models used in the POWER experiment. (left) Domains for the RAP and truncated New England area HRRR for POWER retrospective simulations, with the RAP 13-km-resolution domain in red and the HRRR 3-km-resolution domain in green. (right) Domains for the NAMRR 12-km-resolution parent are shown in black and 4-km-resolution NAMRR CONUS nest in red.

A primary purpose of the HRRR is to improve the operational capability of forecasting high-impact convective storms, which play an important role in the ramping up of low-level winds. With severe data storage limitations, a truncated version of the HRRR domain covering the northeastern United States was used for the POWER study. The version of the HRRR in development during POWER did not perform its own data assimilation on the 3-km grid, but obtained its initial and boundary conditions through direct interpolation from the RAP 13-km grid. The HRRR was run hourly, out to 12 h, within ESRL's high-performance computing facility. The bottom section of Table 3 summarizes the HRRR model configuration, and a more complete HRRR description can be found online (http://ruc.noaa. gov/pdf/HRRRProgramReview-Mar2012.pdf).

We note that after completion of the POWER project, both the RAP and HRRR have switched their model physics to the Mellor–Yamada–Nakanishi–Niino

(MYNN) PBL and surface layer schemes. These new parameterization schemes have resulted in improved low-level wind forecasts over land but have not yet been thoroughly evaluated over water.

b. NAMRR and NAMRR CONUS nest

The NAM (Rogers et al. 2014) serves as the National Weather Service's regional short-range NWP system, which provides forecasts out to 84 h four times a day at 0000, 0600, 1200, and 1800 UTC. Substantial development during the POWER project was undertaken to adapt this model to run on an hourly basis (NAMRR). NAMRR featured two domains (Fig. 3, right): a parent 12-km domain and a one-way nested 4-km domain covering the CONUS. The general configurations of the parameterization schemes used in both the 12- and 4-km domains may be found in Table 4.

We note that after completion of the POWER project, the NAMRR CONUS nest has been moved

TABLE 3. The 13-km RAP and 3-km HRRR domain configurations for POWER.

Model	Configuration
13-km RAP description, CONUS domain subset	
Points in x, y, z directions	758, 567, 51
Microphysics parameterization	Thompson et al. (2008)
Boundary layer parameterization	Janjić (2001)
Convective parameterization	Grell 3D/Grell shallow cumulus
Long/shortwave radiation parameterization	Chou and Suarez (1994), Mlawer et al. (1997)
Land surface model	Smirnova et al. (1997, 2000)
3-km HRRR description truncated from the whole domain	
Points in x, y, z directions	(Truncated to) 520, 450, 51
Convective parameterization	Turned off

TABLE 4. The 12-km NAMRR and 4-km NAMRR CONUS nest domain configurations.

Model	Configuration
12-km NAMRR parent description	
Points in x, y, z directions	954, 835, 60
Microphysics parameterization	Ferrier et al. (2002, 2011)
Boundary layer parameterization	Janjić (2001)
Convective parameterization	Janjić (1994)
Long/shortwave radiation parameterization	Iacono et al. (2008), Mlawer et al. (1997)
Land surface model	Ek et al. (2003)
Gravity wave drag parameterization	Alpert (2004)
4-km CONUS nest description	
Points in x, y, z directions	1371, 1100, 60
Convective parameterization	Janjić (1994); modified to be less active for higher resolution
Gravity wave drag parameterization	None

to a 3-km grid spacing, is fully convection allowing, and, alongside the 12-km domain, has had significant updates to the Ferrier–Aligo microphysics scheme (Aligo et al. 2014).

c. Data assimilation procedure

Both the RAP and NAMRR parent/CONUS nest forecast systems employed in POWER used the Gridpoint Statistical Interpolation (GSI) data assimilation system (Wu et al. 2002).

For the NAMRR, data assimilation is performed on both the 12-km parent and 4-km CONUS nest domains. Assimilation cycles are separated into two types of categories: catch-up and hourly (Fig. 4). Catch-up-type cycles occur at 0000, 0600, 1200, and 1800 UTC and their data assimilation procedure begins at the advertised cycle time (e.g., 1200 UTC) minus 6 h (TM06; e.g., 1200 UTC − 6 h, or 0600 UTC). At TM06 the first-guess atmospheric state provided to the analysis system is from a 6-h forecast from a global atmospheric model; in the case of POWER, this is

the CFSR. Land states are cycled from the previous catch-up cycle's forecast from TM01 (Fig. 4). This practice of regularly resetting the atmospheric state, but fully cycling the land states, is also known as partial cycling and was implemented in the operational NAM forecast system in December 2008 (Rogers et al. 2009).

During the catch-up cycle, hourly analyses are performed over the course of 6 h until TM00, when the free forecast is issued. In the case of POWER, the free forecast at the end of a catch-up cycle is a 36-h forecast for both domains (Fig. 4). The free forecast at the end of the catch-up cycle also provides the 1-h background forecast for the analysis for the second category, the hourly cycle. During the hourly cycle, an analysis and forecast is issued for each hour that is not an advertised catch-up cycle (i.e., 0100–0500, 0700–1100, 1300–1700, and 1900–2300 UTC). Hourly type cycles feature forecasts out to 18 h for both NAMRR domains.

The major difference of the Rapid Refresh system is that this cycling works only for the low-resolution RAP
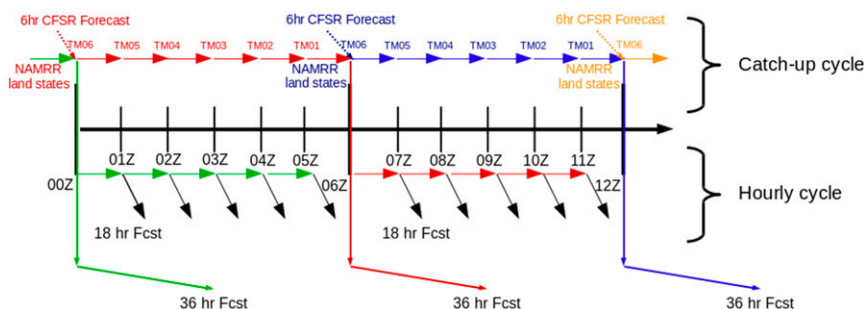

FIG. 4. The data assimilation cycling procedure used in the NAMRR system for the POWER project. The indications of TMXX refer to the current cycle time minus XX hours, e.g., TM06 for a 1200 UTC cycle would be 0600 UTC. The colors denote a continuous thread of cycling, which begins by using the land states from the previous catch-up cycle's forecast from TM01 and a 6-h forecast from the CFSR as the first guess for the atmospheric state at TM06. This procedure is known as the partial cycling; i.e., the land states are continuously cycled but the atmospheric state is not.
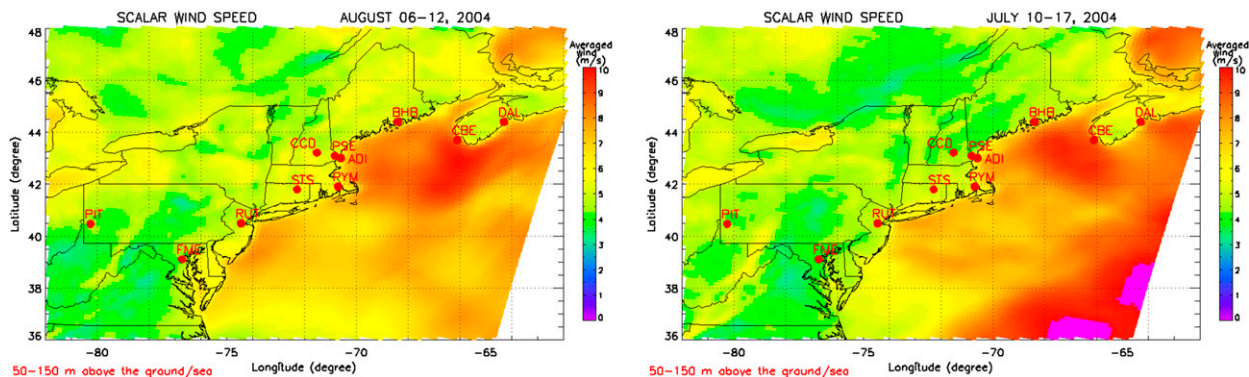
FIG. 5. Scalar wind averaged at 50–150 m AGL/ASL of the RAP model over the two selected time periods: (left) 6–12 Aug and (right) 10–17 Jul, both from the control runs.

model, which is then simply interpolated to the high-resolution HRRR at initialization. That cycling scheme worked at the time of the POWER experiment but later an initialization cycling scheme was incorporated into the operational HRRR model. Also for the RAP used in the POWER project, the CFSR is used twice daily in its own partial cycling procedure (at 0900 and 2100 UTC, starting at 0300 and 1500 UTC) to "reset" the background atmospheric fields, while continuously cycling the RAP soil fields.

For the POWER simulations all models assimilated standard conventional meteorological observations and the NAMRR assimilated satellite radiance observations available to it in 2004. As mentioned before, the experimental runs also assimilated the 11 inland WPRs. Observation errors for all data types were set to match those used in operations, with the exception of the WPR observation type based upon prior experimentation with assimilating WPR data for wind energy applications (Wilczak et al. 2015). WPR observation error standard deviations for the multiagency profiler observations were set to $2 \, \text{m s}^{-1}$ from the surface to 700 hPa. At 700 hPa the error was specified to increase by $0.2 \, \text{m s}^{-1}$ every 50 hPa up to a maximum of $5 \, \text{m s}^{-1}$.

d. Model performance in the Gulf of Maine study region

The map of the U.S. offshore annual wind resource at 90 m above the surface (Schwartz et al. 2010) shows that the Gulf of Maine is a high-resource region with averaged scalar winds mostly greater than $9 \, \text{m s}^{-1}$. We performed a similar analysis for the two time periods chosen for the POWER experiment (Fig. 5).

The wind speed near turbine height (from the third level of the RAP model, approximately 85 m AGL) for these time periods shows the Gulf of Maine as being a good resource for offshore wind during the POWER

experiment time frame, with the mean wind speed typically ranging from 8 to $9 \, \text{m s}^{-1}$ (Fig. 5). For the August study period the overall wind was higher with an average scalar speed of $8.5 \, \text{m s}^{-1}$ at the third RAP model level over the Gulf of Maine area compared to $8.2 \, \text{m s}^{-1}$ in July. The highest wind resources are indicated in the southeast area of the Gulf of Maine, where 95% of the time the speed was greater than $6 \, \text{m s}^{-1}$ (12 kt). We also note that offshore in the Gulf of Maine there is an insignificant difference between the daytime and the nighttime wind speeds, but in the vicinity of the shoreline the daytime wind is stronger at $\sim 6.8 \, \text{m s}^{-1}$, compared to the weaker nighttime wind of $\sim 6.4 \, \text{m s}^{-1}$ (not shown).

4. Model comparisons at the inland wind profiling radar sites

We first determine the impact of assimilating the WPRs at the land-based WPR sites, and second at the *RHB* using the ship's WPR and lidar. The evaluation at the land-based WPR sites is done with the same WPR data that were assimilated in the models. As a metric for measuring the impact from the assimilation of these additional instruments, we use the root-mean-square error (RMSE) of the scalar and vector winds for the control and experimental simulations over the lowest 2 km of the atmosphere. The vector wind RMSE is calculated from the (U, V) components of the wind and indirectly evaluates the wind direction performance in the model.

For the RAP and HRRR, the predicted values were extracted using a parabolic interpolation in the horizontal over the nearest 16 grid points to the profiler site locations. For the NAMRR parent and CONUS nests the vertical profiles were extracted for the model grid point nearest to the profiler locations; this is the same
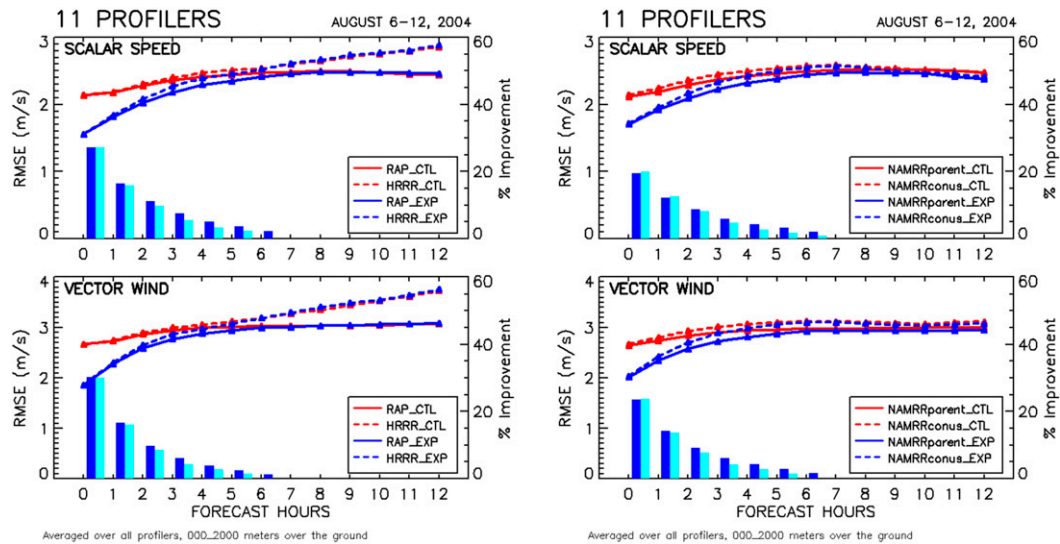
FIG. 6. Land-based WPR RMSEs for the August period. RMSE statistics are shown as a function of forecast lead time for (left) RAP/HRRR and (right) NAMRR models, averaged up to 2000 m AGL. The experimental model runs (in blue) show lower RMSEs compared to the control runs (in red) at the initial time and up to 5–6 h into the forecast. The low-resolution models (RAP and NAMRR parent) are shown with the solid lines, and the high-resolution models (HRRR and NAMRR CONUS) are shown with dashed lines. The bar plots show statistically significant forecast improvements: blue for the low-resolution models and cyan for the high-resolution models. The values of improvement correspond to the right-hand y axis (in %).

method used to provide model sounding data in operations (i.e., BUFR soundings). Following the extraction of the profiles, the model values were then linearly interpolated vertically to the heights of the observed data. Forecasts are evaluated over a 12-h period following initialization.

The RMSE as a function of the forecast hour is shown in Fig. 6 for the August week. In this figure, control runs are in red, and experimental runs are in blue. The NAMRR forecasts are 18 h in length, but they were truncated to 12 h in the following images to make them comparable to those from the RAP and HRRR models. Results from the low-resolution models, along with the RAP and NAMRR parent nests, are shown with solid lines and the high-resolution HRRR and NAMRR CONUS nests are shown with the dashed lines. The bar-plot data present the statistically significant (95% confidence level) improvements of the experimental runs compared to the control runs in percentages as (ControlRMSE − ExperimentalRMSE)/ControlRMSE, with the blue bars indicating the low-resolution model improvements and cyan showing the high-resolution model improvements. The largest improvements in RMSE for the experimental runs versus the control runs are, unsurprisingly, visible at the initial time (forecast hour 0), decreasing at later forecast hours. The noticeable degradation of the HRRR model compared to the RAP model for forecast hours 6 and later could be explained by

the very small truncated domain, which should limit forecast quality beyond the time it takes for flow originating at the lateral boundaries to reach the area at which the model is validated.

In general for the August period, the RMSE improvement for the experimental runs compared to the control runs remains positive through the first five to six forecast hours for all models (Fig. 6). The assimilation of WPR data thus helps to improve the model forecasts locally, at the 11 WPRs, for several hours. Similar results were found for the Wind Forecast Improvement Project (WFIP), as reported by Wilczak et al. (2014, 2015).

The statistics are less positive for the July time period (Fig. 7). Both models showed significant differences in RMSE between the experimental and control runs, for all forecast hours, with the profiler assimilation effects switching to degradation after the first two forecast hours.

Examination of the statistics for each individual day during the July period reveals that the forecast degradation was due to three days of simulations: 13–15 July 2004. Further analysis shows that these three days featured a short-wave trough at midlevels with an associated surface low pressure system passing through the Gulf of Maine, with easterly flow north of the low. One example of this feature is shown in Fig. 8 with the wind field from the RAP model control run in red and the RAP model experimental run in blue, averaged over the lowest 500 m, together with the inland WPRs wind
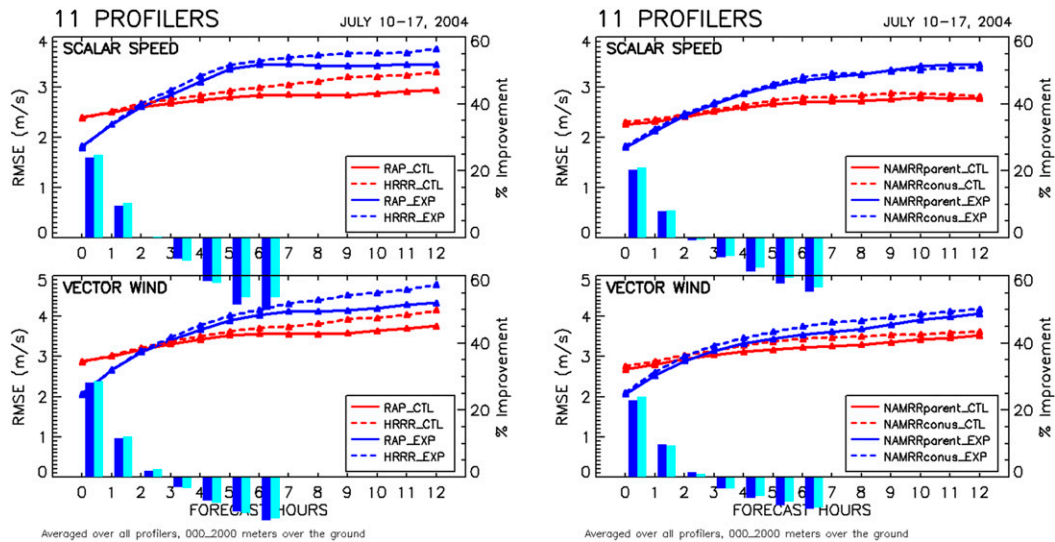
FIG. 7. As in Fig. 6, but for the July period.

data in the same horizontal slice in magenta and the buoy data close to the ocean (~5 m over sea level) in green. The data are shown at 2300 UTC 14 July for forecast hour 0 (Fig. 8, top) and at 0500 UTC 15 July for forecast hour 6 (Fig. 8, bottom). The low pressure system is manifest as a wind vortex in at least the lowest part of the atmosphere, in or close to the Gulf of Maine. Compared to the RAP control run, the experimental run slightly displaced the main vortex but also depicts a second vortex farther southeast in the open ocean (Fig. 8).

It is important to note that similar wind field behavior during the same time frame was found in both of the NAMRR models, with the NAMRR experimental runs also creating two separate vortices from the beginning of the runs. To examine this event in more detail using available observations, we considered a dataset of buoy observations that provides wind speed measurements at 2–6 m above the ocean surface (Fig. 9). The map of the buoy locations is in the left panel of Fig. 9. We separated the buoys into three sets: one set includes the buoys along the coast (cyan in the left panel of the figure), the second set is in the central part of the Gulf of Maine (orange in the same panel), and the third set includes the buoys farthest from the coast (magenta in the same panel).

We compared the buoy data to the model values at these locations, at the initialization time for the first level of the model, which is slightly greater than 10 m above sea level (RAP 11 m, NAMRR 20 m). We calculated the RMSE statistics using the three buoy sets and present the results in the six middle and right panels of Fig. 9. The RAP model is in the middle and the NAMRR model is on the right, with control runs colored in red and experimental runs colored in blue. The times of largest discrepancy

between the experimental and control runs are highlighted in the circles. These large differences occur only for the set of buoys farthest from the coast. Moreover, both models show the same "problematic" days of 13–15 July 2004, when the model experimental run has larger RMSEs than the control run. This suggests that the atmospheric regime away from the coast was not well sampled, but does not completely explain why the addition of WPR data in the experimental run would lead to forecast degradation relative to the control run. To more completely address this question, the WPR observations over that period are investigated.

In Fig. 8 it is noted that the synoptic low produced easterly winds through the Gulf of Maine. To understand how model skill is affected as a function of WPR location for the problematic July period, the profiler data from the lowest range gates are shown in Figs. 10 and 11 (for forecast hours 0 and 6, respectively). The sites were separated into three sets: one set includes the profilers along the coast (cyan in the left panel of Fig. 10), the second set features the profilers slightly farther from the coast of the Gulf of Maine (orange in the same panel), and the third set includes the profiler farther inland (magenta in the same panel). The RAP model output is shown in the three central panels, and the NAMRR model values are in the three right panels, with the control runs in red and the experimental runs in blue. Here, we see that, as expected, the RMSE of the experimental runs is smaller compared to the RMSE of the control runs for all sets of radars and for both models at the model initialization time (forecast hour 0).

The same statistics, but for forecast hour 6, show the experimental run being worse compared to the control
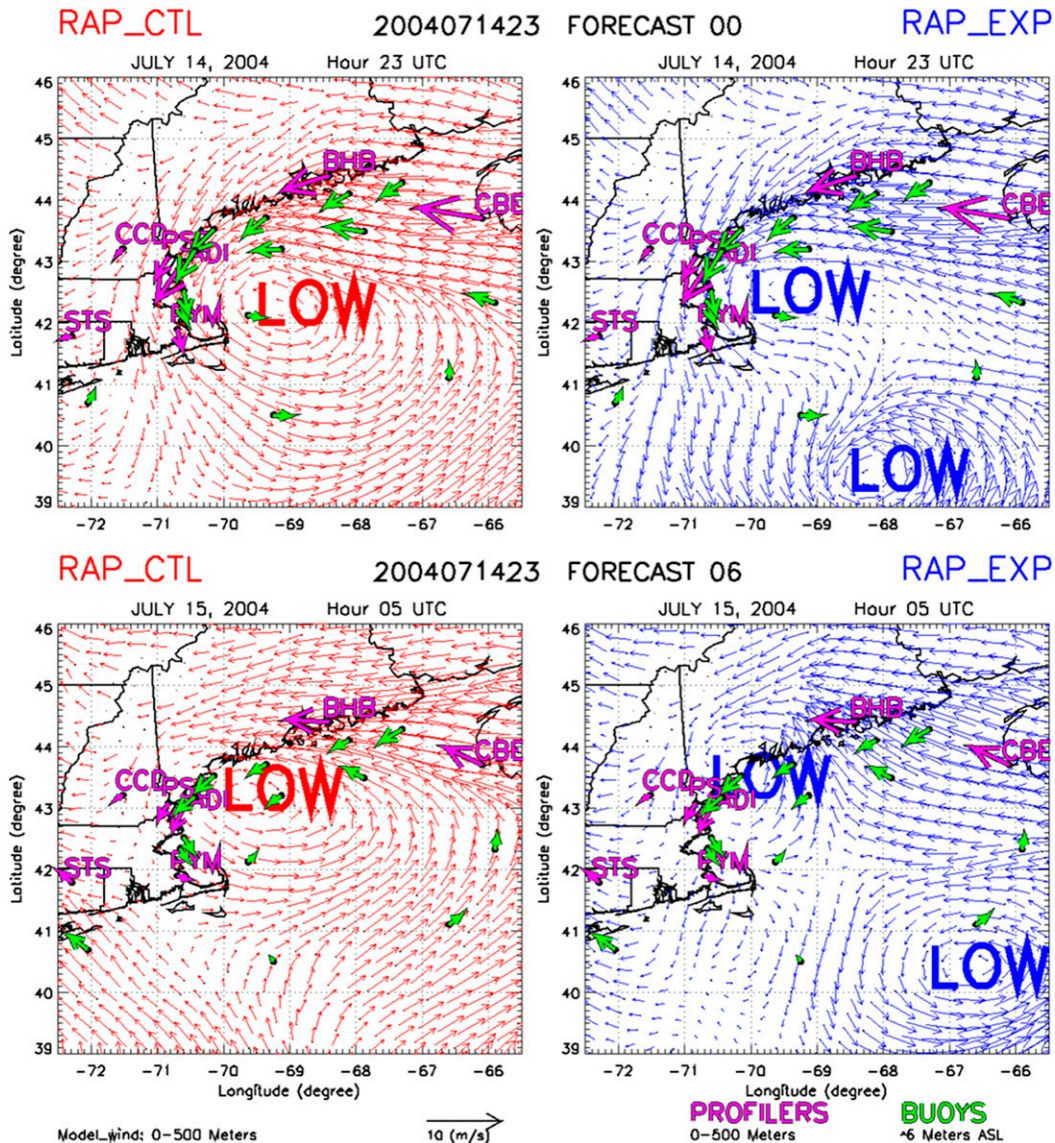
FIG. 8. RAP model output data for the (left) control (red) and (right) experimental (blue) runs. Winds are averaged over 500 m above the surface at (top) 2300 UTC 14 Jul, at the model initialization time, and (bottom) at 0500 UTC 15 Jul, at forecast hour 6. Also the buoy data at 2–5 m ASL are shown in green, and the radar data averaged over 500 m above the surface are shown in magenta.

run (Fig. 11). The statistics present discrepancies between the experimental and control runs for the known problematic days of the July time period, 13–15 July. The three center and right panels in Fig. 11 show that this discrepancy mostly occurred for the profilers located along the coast of the Gulf of Maine (as highlighted by the black circles).

This supports what we had found from the buoy analysis: that the degradation in the experimental run was, in part, due to the undersampled easterly forcing present over the ocean for those particular days. This

undersampling is likely exacerbated by the profiler data provided in the experimental run; that is, the profiler network is only partially resolving the winds associated with the synoptic low in the Gulf of Maine. This partial (under-) sampling of easterly flow is hypothesized to have led to an aliasing issue in the analysis. In addition, further investigation of the Appledore Island, Maine, WPR data (ADI; Figs. 1 and 12) during the problematic time periods of 13–15 July revealed that the wind direction changed to the onshore directions of south, southeast, and east. This is in contrast
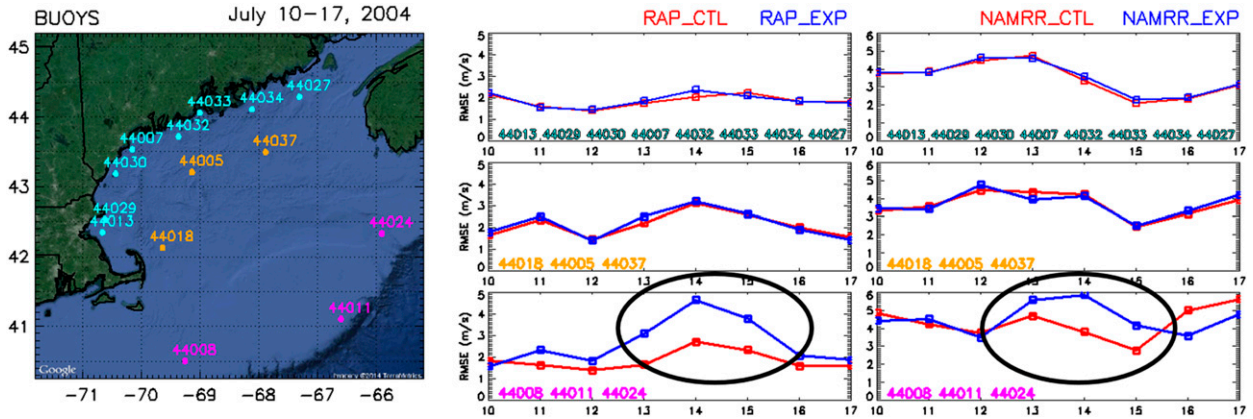
FIG. 9. (left) Locations of the buoys, separated into three sets: along the coast, cyan; in the center of the Gulf of Maine, orange; and far offshore, magenta. The corresponding RMSE statistics for the (center) RAP and (right) NAMRR models, over the eight days during the July period, at forecast hour 0, (top) along the coast, (middle) in the center of the Gulf of Maine, and (bottom) far offshore.

to the other days, when westerly or northerly wind directions offshore flow prevailed, thus making the impact of the inland-located WPRs more significant.

While it is not generally expected, the assimilation of new observations can have a negative impact on forecasts. Both Morss and Emanuel (2002) and Semple et al. (2012) found that it is not unusual for assimilated observations to have the potential to degrade the analysis and forecast on occasion. The impact of assimilated observations is sensitive to the forecast model, the quality of the observations, how well the atmosphere is observed, and the assimilation methodology. Given that all forecast models in the experimental run showed degradation, in addition to the thorough quality control of the WPR data, it is most likely that the degradation is a combined result of insufficient sampling during an easterly flow atmospheric regime and the assimilation methodology.

Figure 1 shows that the network of the 11 WPRs is restricted to the northeast coast of the United States, in an approximately linear configuration, with no WPRs residing farther offshore. As noted in the buoy analysis, WPR analysis, and investigations of the ADI observations, it appears likely that the WPRs only partially sampled the onshore flow associated with a westward-moving surface low (Fig. 8). It is hypothesized that in such a situation this incomplete sampling leads to aliasing in the analysis (i.e., overfitting of the experimental WPR data in the Gulf of Maine). We further hypothesize that this effect was exacerbated by the lack of flow dependence in the background error covariance associated with the three-dimensional variational data assimilation (3DVAR) approach employed within this study. The specification of the background error is important, as it determines how the information from the observations is spread out into the analysis. With the
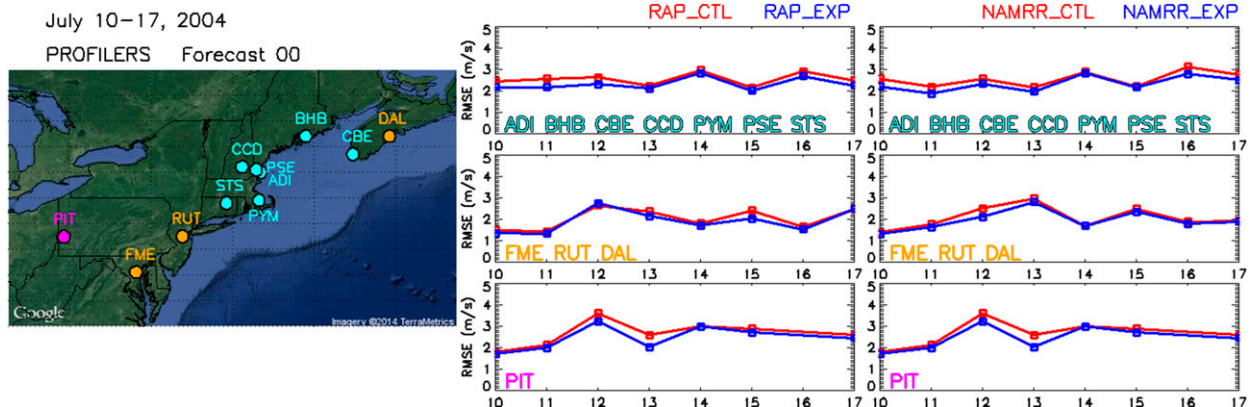

FIG. 10. (left) Map of the profiler locations, separated into three sets: onshore bordering the Gulf of Maine, cyan; other coastal locations, orange; and far inland (only one profiler in Pittsburgh, PA), magenta. Corresponding RMSE statistics are shown for the (center) RAP and (right) NAMRR models, for the July period. The model outputs are compared at forecast hour 0.
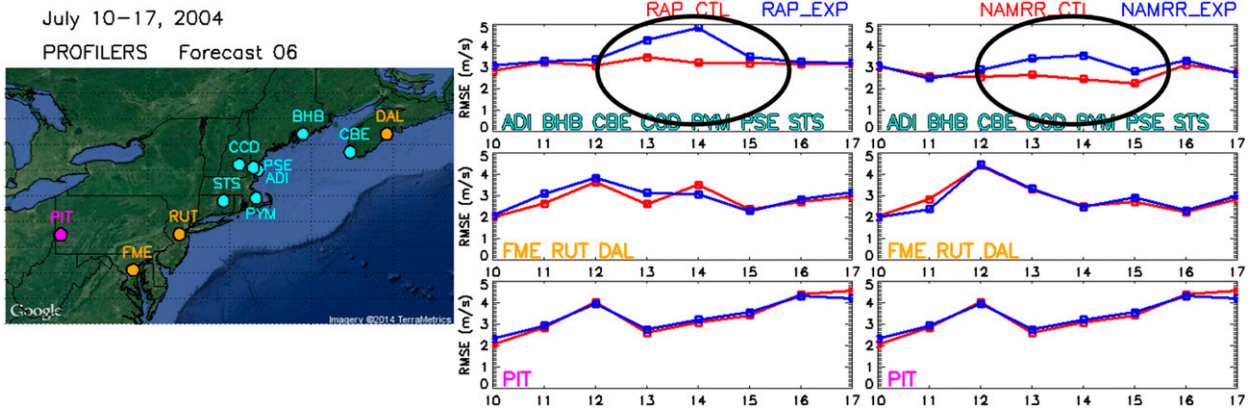
FIG. 11. As in Fig. 10, but for forecast hour 6. The circled areas in the RAP and NAMRR time series highlight the periods of forecast degradation associated with the July study period.

3DVAR scheme employed here, all systems used background error covariances associated with their operational counterparts at NCEP. This background error is a climatological estimate and is static (i.e., unchanging), therefore missing the so-called errors of the day (Lorenc 2003; Kalnay 2003). A more advanced assimilation technique that provides flow-dependent, multivariate background errors (e.g., ensemble-based methods) would likely have made better use of the

assimilated data, possibly improving the results. Unfortunately those updated techniques could not be used for the POWER project because of the lack of available GFS Global Data Assimilation System (GDAS) ensemble Kalman filter (EnKF) members for 2004, which both the RAP and NAMRR/CONUS nest systems now use as a part of a hybrid ensemble–3DVAR analysis.

For this type of meteorological situation, the availability of more offshore observations, such as buoy-mounted
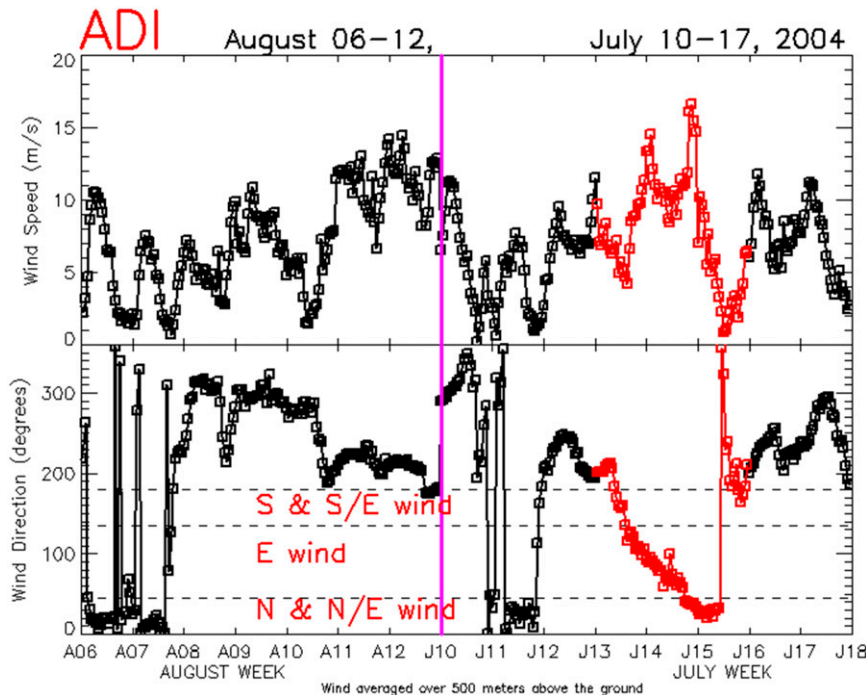

FIG. 12. ADI WPR (top) wind speed data and (bottom) wind direction. Data are averaged over 500 m AGL for all POWER project days, with the (left) August and (right) July days shown. The red-colored section indicates the easterly flow observed during the problematic time period of 13–15 Jul 2004.
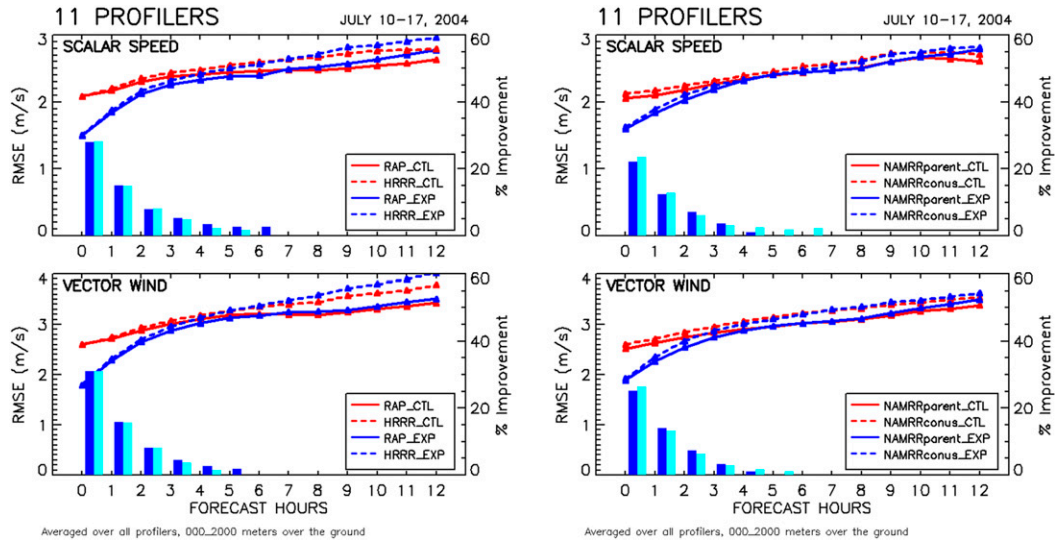
FIG. 13. As in Fig. 6, but excluding the following sites around the Gulf of Maine on the following days: 13 Jul—ADI, BHB, CBE, CCD, PSE, PYM, and STS; 14 Jul—ADI, BHB, CBE, CCD, PSE, PYM, and DAL; 15 Jul—BHB, CBE, DAL, and PYM.

wind profiling systems, might have ensured sufficient sampling of the atmosphere and have provided better constraints on the model at the initialization time, possibly yielding a better forecast. A similar finding was made in the WFIP experiment (Wilczak et al. 2015) but is much more difficult to fulfill experimentally in an offshore region.

We reran the statistical analysis presented in Fig. 7 but excluding those sites over the 3-day period that were influenced by the westward-propagating synoptic low pressure system. In particular, seven sites (ADI, BHB, CBE, CCD, PSE, PYM, and STS) were excluded on 13 July 13, seven sites (ADI, BHB, CBE, CCD, PSE, PYM, and DAL) were excluded on 14 July, and four sites (BHB, CBE, DAL, and PYM) were excluded on 15 July. The results are presented in Fig. 13. When those data were removed from the analysis, the rest of the July days behaved much like the August period, where the experimental runs showed large RMSE improvement at the initialization time both for scalar and vector winds, remaining positive through the first five to six forecast hours for all models. From this analysis we can conclude that in general assimilating the WPR data improved the model forecast for a few to several hours.

5. Model comparison with the *RHB* data

a. Wind profiling radar

To complete the analysis of how the assimilation of the data from the 11 land-based WPRs impacted the forecast, we next use the data collected by the *RHB* WPR and compare them to the same models used in the

preceding analysis. The ship track was presented earlier in Fig. 2. The model predictions are extracted at the moving location of the ship on an hourly basis. An example of a time–height cross section of the observed wind, together with results from all four model control runs, is shown in Fig. 14 for 7 August 2004, at the model initialization time. In contrast to the 11 inland WPRs, the *RHB* WPR data were not assimilated into the models and are used only for validation. The visual comparison reveals obvious commonalities in both wind direction and wind speed between the observed and modeled data. Thus, the wind direction changes from northerly or northeasterly at the beginning of the day to northwesterly in the middle of the day, and finally to southwesterly; low wind speeds are present in the first 5–6 h of the day for the lowest 500 m ASL, increasing in strength when the direction changed. A tiny slice of very low wind speed is present at the altitude of ~3000–3300 m ASL. Finally, the wind speed has noticeably increased by the end of the day in the lower levels of the atmosphere. All these phenomena are observed and present more or less in all of the models.

For the August and July analysis periods, we compare the observed mean scalar wind profiles of the *RHB* WPR with the mean scalar wind profiles of the models up to 4 km ASL at forecast hour 0. In Fig. 15 we show the comparison of the WPR observations versus the RAP/HRRR (control and experimental runs) models in the left panels and the comparison of the observations versus the NAMRR parent/CONUS (control and experimental runs) models in the right panels for the two time periods (the August period is presented on the top and
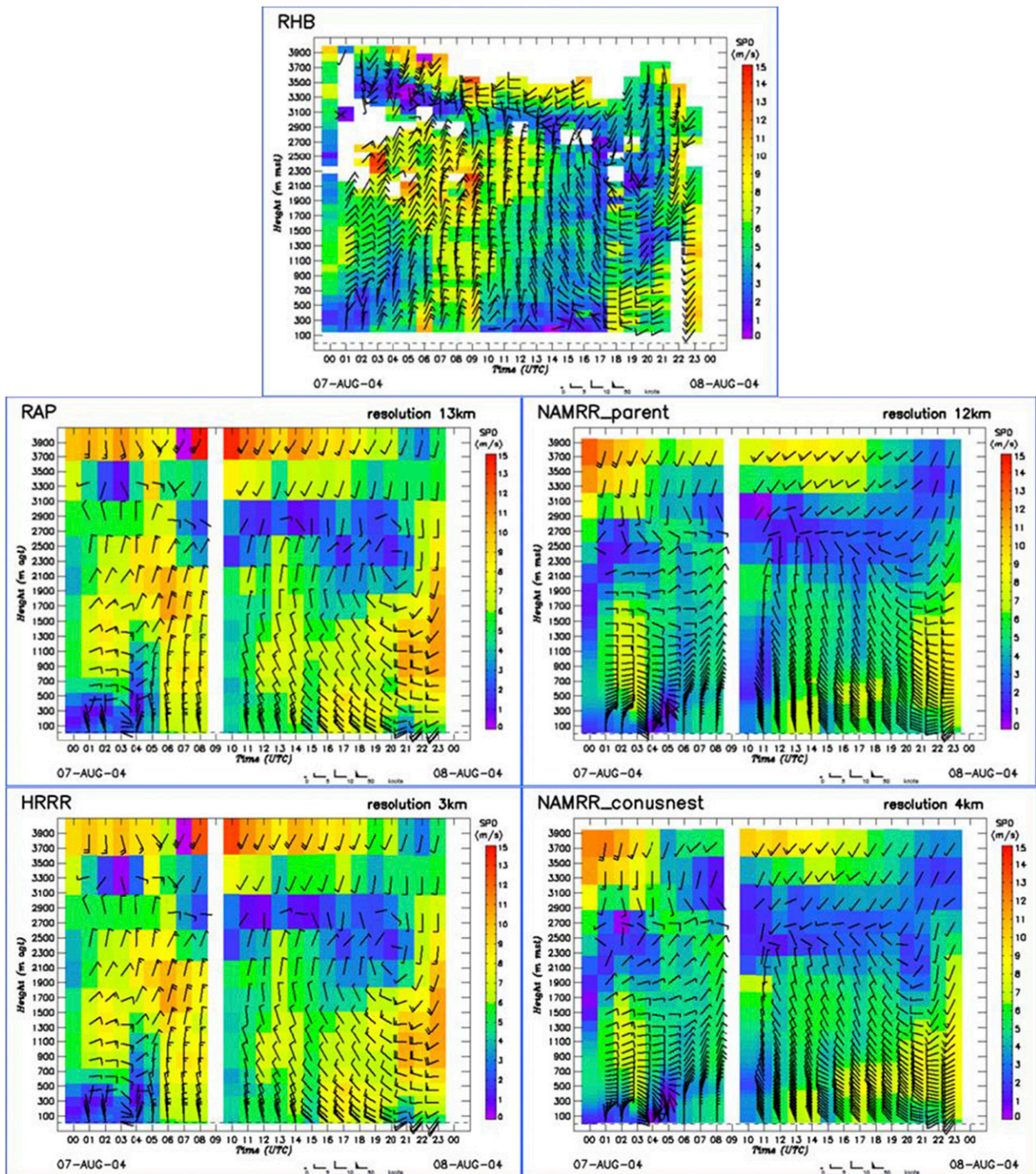
FIG. 14. Time–height cross sections of WPR-measured and modeled winds for 7 Aug 2004. Shown are data for (top) *RHB* WPR, (left) RAP/HRRR, and (right) NAMRR parent/CONUS nests. The model output shown is a concatenation of all hour 0 forecasts.

July is on the bottom). The July dataset includes 5 days only, as we exclude 13–15 July from this analysis as well. We note that in general the experimental runs are in closer agreement with the observations.

We have shown that the assimilation of wind profiles from 11 inland WPRs improves the model wind speed

forecast averaged over the lowest 2 km at the WPR locations for several forecast hours from the initialization time. Since wind turbines are likely to be sited offshore, it is natural to ask if this improvement extends to the offshore area using independent data for verification (i.e., *RHB* WPR observations). For this purpose the
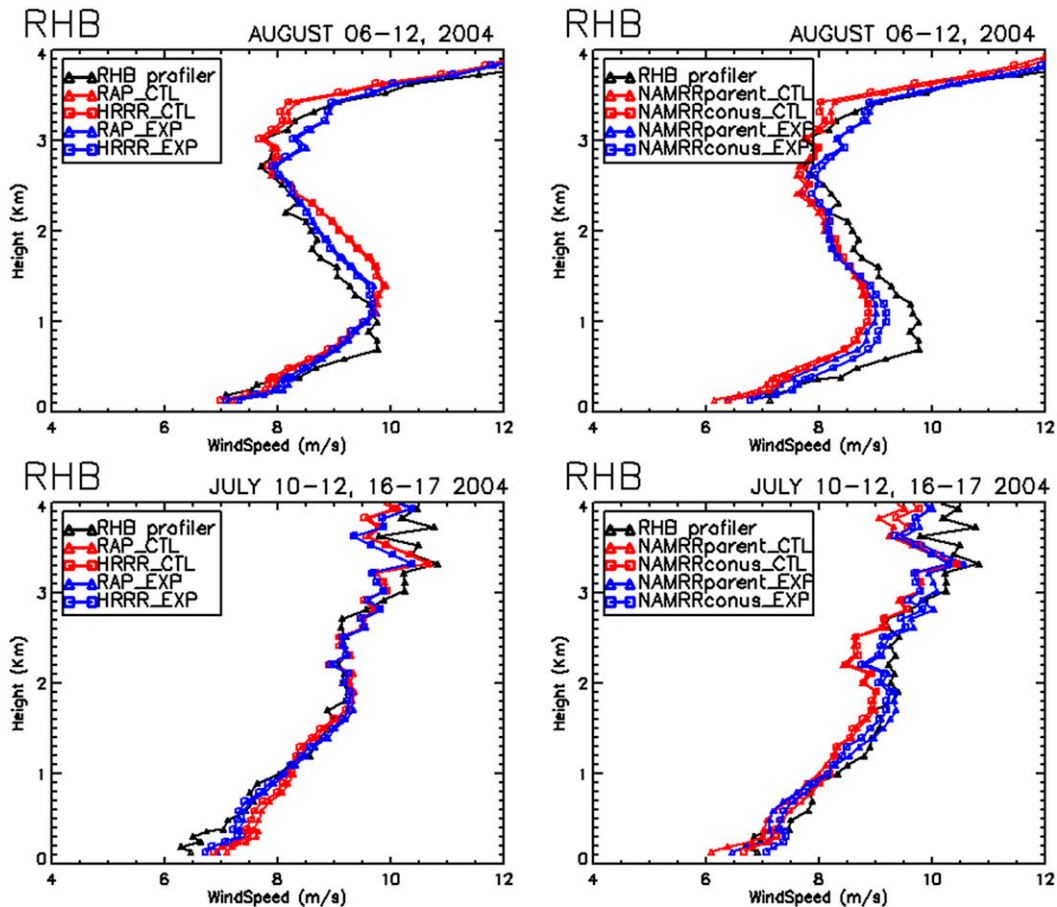
FIG. 15. Scalar wind profiles of observations and models up to 4 km ASL, averaged over the two chosen periods: (top) August and (bottom) July. Comparisons of (left) RAP/HRRR models and WPR observations and (right) NAMRR parent and CONUS models. The model outputs are compared at forecast hour 0.

same statistical analysis has been done using the observed data from the *RHB* WPR and the model values extracted at the *RHB* locations within the Gulf of Maine. Figure 16 displays the RMSE statistics for the RAP/HRRR (experimental and control runs) models on the left and the NAMRR parent/CONUS (experimental and control runs) models on the right. The dataset used here combines the August and July periods, but is limited to 12 days of offshore flow only (13–15 July are again excluded). RMSE values are computed over the first 2 km of the atmosphere. From this plot it can be seen that the experimental runs have improved RMSEs compared to the control runs, particularly over the first four to seven forecast hours for the RAP/HRRR models and much longer for the NAMRR parent/CONUS nests. The fact that the improvement persisted for a considerable number of forecast hours is further illustrated in the bar plots inserted into the figures, showing the values of the percent RMSE improvement that are statistically significant at the 95% confidence level.

The WPR analysis shown so far demonstrates a positive impact from the assimilation of the 11 onshore WPRs. The positive impact is evident on both model datasets extracted at the inland radar locations as well as on the independent *RHB* WPR. At forecast hour 1 the impact of the assimilation reduces the RMSE by 12%–18% at the inland locations and by 5%–8% on the *RHB* ship track. During the next several forecast hours this improvement decreases quickly but is still indicated up to 5–6 h into the forecasts.

b. Doppler lidar

To focus more on forecasts at the heights of the offshore wind turbines, the model values have to be evaluated in or near the expected turbine layer: 90–100 m above the ocean. For this purpose HRDL data measured on the *RHB* are used.

Two HRDL examples with different types of wind features are shown in Fig. 17 (scalar winds are in color and vector winds are shown by arrows), for 10 August (right) and 12 July (left). The time–height cross sections
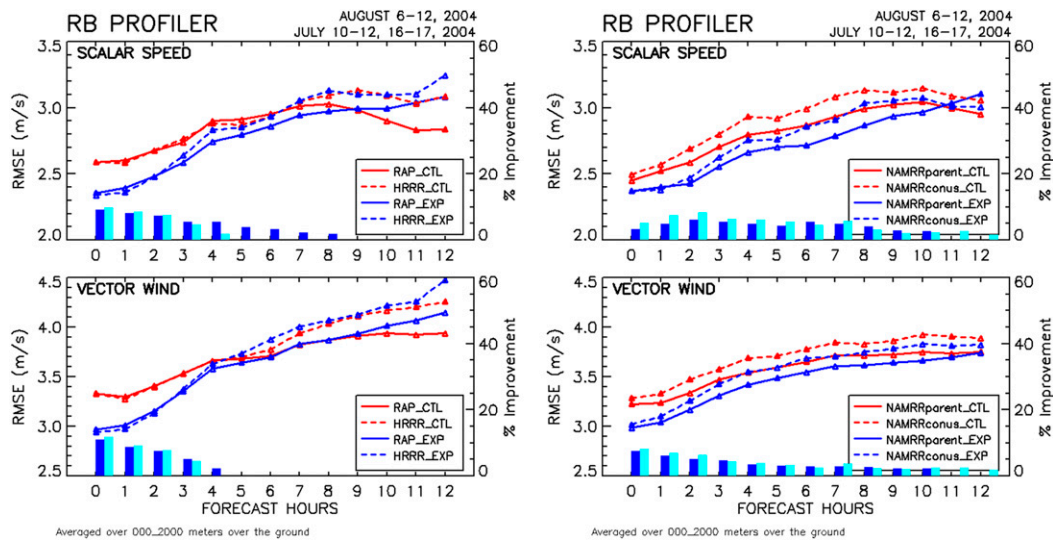
FIG. 16. As in Fig. 6, but for the *RHB* WPR, over 12 days from both analysis periods.

of the HRDL-measured wind speed data (Fig. 17, top left and right) are plotted against RAP model data at forecast hour 2 for 10 August and at forecast hour 1 for 12 July for the control and experimental runs. At the bottom of Fig. 17, the turbine-height time series of the wind averaged from 50 to 150 m AGL is shown. Visual inspection of both sets of panels shows a good level of agreement for both the RAP vertical profiles simulations and the RAP/HRRR time series with the HRDL data. In several time–height areas the experimental runs are closer to the observed wind speeds than the control runs: the high-wind ramp up from the control runs at 2000 UTC 12 July 2004 is not observed and is shown with smaller magnitude in the experimental runs; on the other hand, the observed 8–9 m s^{-1} winds at 100–200 m ASL during 0400–0600 UTC 10 August 2004 are present in the experimental runs but are not visible in the control runs, demonstrating that the positive impact of assimilation of the onshore WPRs extends to offshore locations.

To evaluate in detail the direct impact of the assimilation of the onshore WPRs data for wind energy purposes, a layer of the HRDL and RAP/HRRR model data from 50 to 150 m above the ocean has been extracted and vertically averaged. The model values were then linearly interpolated to the HRDL profile levels and were compared against HRDL data in terms of correlation coefficient, bias, and mean absolute error (MAE). Figure 18 shows HRDL scalar winds compared to RAP control and experimental runs at ship track locations for 6–12 August 2004 at forecast hour 1. First, it is clear how well the RAP model follows the scalar wind variability for the full range of detected winds from 1–2 to 12–14 m s^{-1}. Second, we note that the experimental run has better statistical overall

agreement, including a higher correlation (0.89 for the experimental run vs 0.87 for the control run), lower bias (0.05 vs −0.13 m s^{-1}), and lower MAE (1.11 m s^{-1} from the experimental run compared to 1.23 m s^{-1} in the control run). Third, the visual comparison of the difference between control MAE and experimental MAE (Fig. 18, right) confirms these statistics, with more warm-color (yellow–red) cells of larger control MAE compared to the number of cold-color (blue) cells of larger experimental MAE.

A full statistical analysis of the scalar wind speed correlation coefficients up to forecast hour 3 is presented in Table 5 for the two data periods separated by a solidus (/): first for 6–12 August 2004 and second for the selected dates during the July analysis week, 10–12 and 16–17 July 2004. Both model resolutions (RAP and HRRR) show almost the same correlation coefficient behavior with the highest correlation at forecast hour 1 gradually diminishing at later forecast hours but still higher than 0.7. Up to forecast hour 3, both the RAP and HRRR, as well as the NAMRR CONUS, for the July episode generally have improved correlation coefficients for the experimental versus control runs.

MAE statistics (Table 6) show a larger improvement for the experimental runs compared to the control runs for the high-resolution models (HRRR and NAMRR CONUS) versus the low-resolution models (RAP and NAMRR parent), especially for forecast hour 1. Thus, the experimental versus control improvement for forecast hour 1 reaches 15% for the HRRR during the August time period and 24% for the NAMRR CONUS during the July time period. Overall, the MAE statistics confirm that improvements
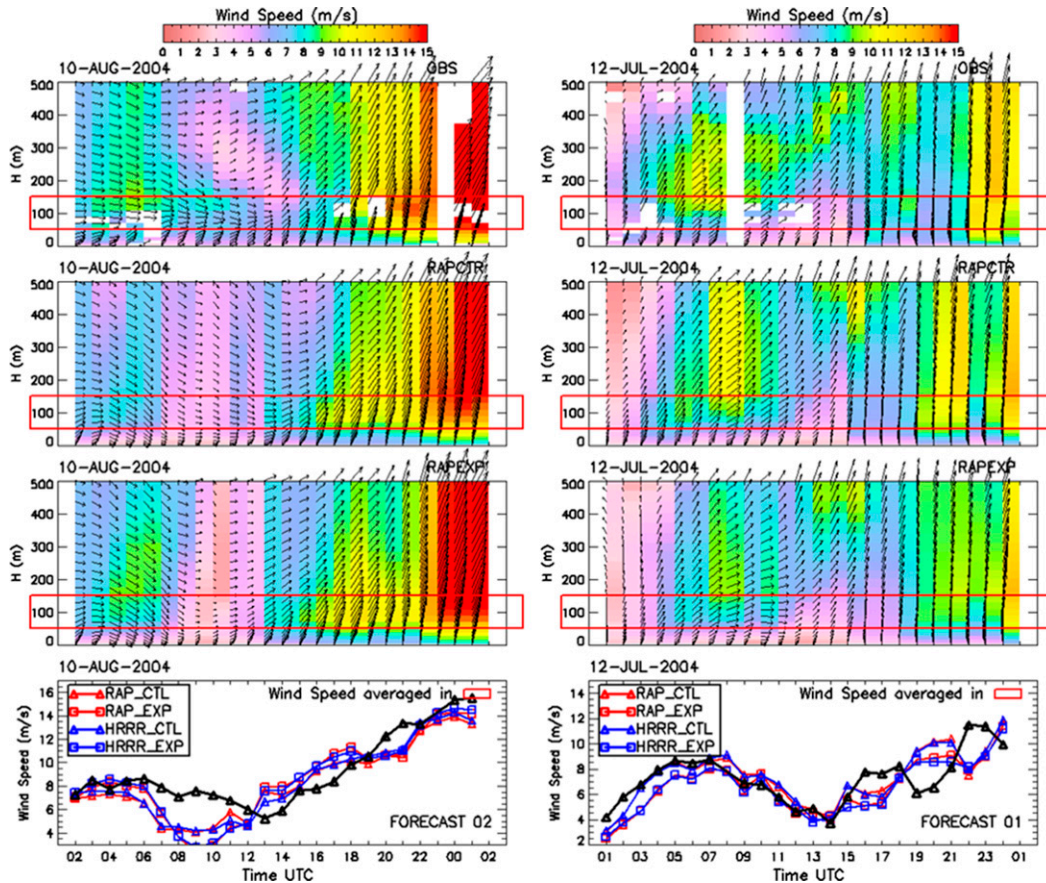
FIG. 17. Time–height cross sections of (first row) 1-h-averaged lidar-measured and (second row) modeled RAP control and (third row) RAP experimental scalar wind speeds (colored contours) and vector winds for (left) 10 Aug and (right) 12 Jul 2004. (fourth row) The turbine-height (averaged from 50 to 150 m AGL) wind speed with the HRDL data in black, RAP model in red, and HRRR model in blue. The control runs are marked with an open triangle and the experimental runs with an open square. The (bottom left) August data are a concatenation of all hour 2 forecasts and the (bottom right) July data are for the hour 1 forecasts.

due to the assimilation of the onshore WPRs data in the offshore area can be retained for up to three forecast hours.

Recently, a similar study has been conducted over two continental U.S. locations in the Great Plains and west Texas: the Wind Forecast Improvement Project (Wilczak et al. 2014, 2015). Despite the fact that the scale of WFIP was markedly larger, the purpose was similar: to improve NWP forecasts by enhancing measurement networks and assimilating supplemental data, including WPRs. The scalar wind speed forecast was improved in both areas with greater improvement in the northern plains area, where more uniformly distributed observational instruments were deployed. For the POWER project the WPRs used for data assimilation were located in a nearly linear alignment along the coast to the west of the *RHB* ship track. This result may partially explain the fact that the

model statistical improvement is, generally, limited to the first four forecast hours and especially to the negative results of assimilation during the three days with easterly onshore wind directions during 13–15 July 2004.

6. Conclusions

Observations from 11 WPRs, deployed near the North Atlantic shore of the United States, collected during the NEAQS experiment of 2004, were used to evaluate the impact of their assimilation in four NWP NOAA models: RAP/HRRR models running at ESRL/GSD and NAMRR parent/CONUS models running at NCEP. The models have been run in two identical configurations except for the assimilation of the 11 inland WPRs at forecast hour 0. To evaluate the
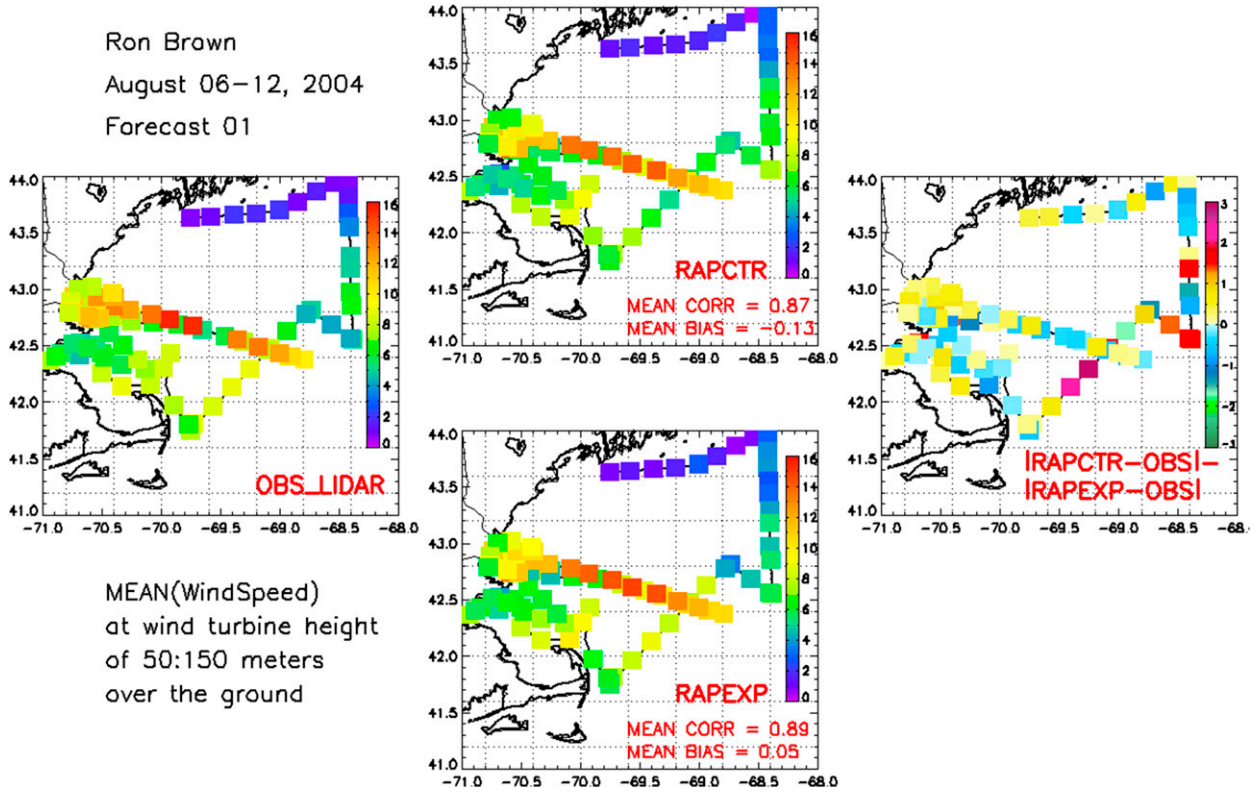
FIG. 18. Offshore scalar wind averaged over the layer 50–150 m. (left) HRDL data, (center) RAP control and experimental forecast hour 1 results with statistical values of correlation coefficients and bias, and (right) the difference between the model errors, calculated as |RAPCTR-HRDL| − |RAPEXP-HRDL|.

impact of the WPR assimilation, the scalar and vector winds were vertically averaged in the layer 0–2 km above the surface and compared against the onshore WPRs data. While it is not surprising that the data from the experimental runs had a closer fit to the observations at the initialization time (~30% improvement compared to the control runs), it is worth noting that the experimental simulations retained some of this positive impact through the first five to six forecast hours. The model

forecasts of offshore winds in the Gulf of Maine were also evaluated where the NOAA Research Vessel *Ronald H. Brown* cruised during the NEAQS-2004 experiment. A ship-based WPR and high-resolution Doppler lidar (HRDL) were used for model evaluation without being assimilated into the models, thus providing a more independent source for verification. The results show a positive impact on the forecast skill at the offshore locations with 3%–10% of the forecast improvement being

TABLE 5. Correlation coefficients R^2 between scalar wind data for the HRDL observations and the four models for the layer between 50 and 150 m ASL. Numbers on the left indicate the data averaged for all hours between 6 and 12 Aug 2004 and numbers on the right indicate the data averaged for all hours between 10 and 12 and 16 and 17 Jul 2004. Boldface numbers mark improved values of the experimental simulations relative to the control simulations.

	Initial	Forecast hour 1	Forecast hour 2	Forecast hour 3
RAP_CTR	0.85/0.92	0.87/0.90	0.84/0.84	0.79/0.81
RAP_EXP	**0.88/0.94**	**0.89/0.92**	**0.86/0.87**	**0.81/0.82**
HRRR_CTR	0.83/0.91	0.87/0.89	0.86/0.85	0.80/0.81
HRRR_EXP	**0.86**/0.93	**0.89/0.92**	**0.87/0.88**	**0.82/0.82**
NAMRRparent_CTR	0.81/0.87	0.87/0.86	0.87/0.81	0.84/0.73
NAMRRparent_EXP	0.81/0.87	0.86/0.86	0.87/0.81	0.84/0.73
NAMRRconus_CTR	0.84/0.86	0.88/0.84	0.86/0.79	0.81/0.75
NAMRRconus_EXP	0.83/**0.89**	0.87/**0.90**	0.86/**0.86**	0.80/**0.78**

TABLE 6. As in Table 5, but for MAEs (m s^{-1}). Data in boldface italics mark statistically significant differences at the 95% confidence level.

	Initial	Forecast hour 1	Forecast hour 2	Forecast hour 3
RAP_CTR	1.33/1.12	1.23/1.15	1.32/1.40	1.53/1.57
RAP_EXP	*1.18/1.07*	*1.11/1.08*	*1.26/1.34*	*1.46*/1.59
HRRR_CTR	1.45/1.22	1.24/1.19	1.25/1.43	1.54/1.57
HRRR_EXP	*1.30/1.12*	*1.06/1.06*	*1.23/1.27*	*1.47/1.49*
NAMRRparent_CTR	1.88/1.88	1.58/1.75	1.39/1.80	1.45/1.95
NAMRRparent_EXP	*1.78/1.75*	*1.52/1.57*	*1.38/1.69*	1.46/*1.87*
NAMRRconus_CTR	1.65/1.60	1.36/1.54	1.36/1.72	1.49/1.82
NAMRRconus_EXP	*1.57/1.39*	*1.33/1.17*	*1.35/1.37*	1.61/*1.61*

observed during the first four forecast hours for the winds up to 2 km above the ocean. Furthermore, forecast improvement was seen in the NAMRR parent/CONUS domains for up to 12 forecast hours at the *RHB* WPR.

To measure the impact for wind energy purposes, the model evaluations were repeated at expected turbine heights (50–150 m above the sea level), but with the HRDL data. Detailed comparisons of the RAP/HRRR and NAMRR parent/CONUS runs with and without the assimilation of 11 inland WPRs showed forecast improvements in offshore areas, at approximate turbine heights, for at least three forecast hours after initialization. High-resolution models (HRRR and NAMRR CONUS) show generally similar statistics when compared to their lower-resolution versions, with slightly better MAEs for the higher-resolution NAMRR compared to the NAMRR parent.

It was also found that events with a negative impact of the WPR data assimilation can occur, and were hypothesized to be a combined effect of the assimilation methodology (3DVAR) and poorly sampled meteorological conditions, especially in the case of easterly onshore flow. These negative impacts might be smaller, or turn positive, if more advanced data assimilation techniques were used. We may speculate that for offshore areas, in general, installing measurement systems on the nearby land may not be sufficient. For some atmospheric conditions such as the observed cyclonic synoptic low, additional profiling data measured over the open ocean are needed. Future efforts should investigate the data assimilation methodology as well as the observing network design, perhaps through an observing system simulation experiment.

REFERENCES

Aligo, E., B. S. Ferrier, J. Carley, E. Rogers, M. Pyle, S. J. Weiss, and I. L. Jirak, 2014: Modified microphysics for use in high-resolution NAM forecasts. *Proc. 27th Conf. on Severe Local Storms*, Madison, WI, Amer. Meteor. Soc., 16A.1. [Available online at https://ams.confex.com/ams/27SLS/webprogram/Paper255732.html.]

Alpert, J., 2004: Sub-grid scale mountain blocking at NCEP. *Proc. 20th Conf. on Weather on Analysis and Forecasting/16th Conf. on Numerical Weather Prediction*, Seattle, WA, Amer. Meteor. Soc., P2.4. [Available online at https://ams.confex.com/ams/pdfpapers/71011.pdf.]

Angevine, W. M., J. E. Hare, C. W. Fairall, D. E. Wolfe, R. J. Hill, W. A. Brewer, and A. B. White, 2006: Structure and formation of the highly stable marine boundary layer over the Gulf of Maine. *J. Geophys. Res.*, **111**, D23S22, doi:10.1029/2006JD007465.

Banta, R., and Coauthors, 2014: NOAA study to inform meteorological observation for offshore wind: Positioning of Offshore Wind Energy Resources (POWER). NOAA Final Tech. Rep. to DOE, Award DE-EE0003080, 145 pp. [Available online at http://www.esrl.noaa.gov/gsd/renewable/AMR_DOE-FinalReport-POWERproject-1.pdf.]

Carley, J. R., and Coauthors, 2015: Ongoing development of the hourly-updated version of the NAM forecast system. *Proc. 27th Conf. on Weather Analysis and Forecasting/23rd Conf. on Numerical Weather Prediction*, Chicago, IL, Amer. Meteor. Soc., 2A.1. [Available online at https://ams.confex.com/ams/27WAF23NWP/webprogram/Paper273567.html.]

Carter, D., K. S. Gage, W. L. Ecklund, W. M. Angevine, P. E. Johnston, A. C. Riddle, J. Wilson, and C. R. William, 1995: Developments in UHF lower tropospheric wind profiling at NOAA's Aeronomy Laboratory. *Radio Sci.*, **30**, 977–1001, doi:10.1029/95RS00649.

Chou, M.-D., and M. J. Suarez, 1994: An efficient thermal infrared radiation parameterization for use in general circulation models. NASA Tech. Memo. 104606, Tech. Rep. Series on Global Modeling and Data Assimilation, Vol. 3, 85 pp. [Available online at https://ia600502.us.archive.org/23/items/nasa_techdoc_19950009331/19950009331.pdf.]

Ek, M. B., K. E. Mitchell, Y. Lin, E. Rogers, P. Grunmann, V. Koren, G. Gayno, and J. D. Tarpley, 2003: Implementation of Noah land surface model advances in the National Centers for Environmental Prediction operational mesoscale Eta model. *J. Geophys. Res.*, **108**, 8851, doi:10.1029/2002JD003296.

Ferrier, B. S., Y. Jin, Y. Lin, T. Black, E. Rogers, and G. DiMego, 2002: Implementation of a new grid-scale cloud and precipitation

scheme in the NCEP Eta model. Preprints, *19th Conf. on Weather Analysis and Forecasting/15th Conf. on Numerical Weather Prediction*, San Antonio, TX, Amer. Meteor. Soc., 280–283.

——, W. Wang, and E. Colon, 2011: Evaluating cloud microphysics schemes in nested NMMB forecasts. *Proc. 24th Conf. on Weather Analysis and Forecasting/20th Conf. on Numerical Weather Prediction*, Seattle, WA, Amer. Meteor. Soc., 14B.1. [Available online at https://ams.confex.com/ams/91Annual/webprogram/Paper179488.html.]

Grund, C. J., R. M. Banta, J. L. George, J. N. Howell, M. J. Post, R. A. Richter, and A. M. Weickmann, 2001: High-resolution Doppler lidar for boundary-layer and cloud research. *J. Atmos. Oceanic Technol.*, **18**, 376–393, doi:10.1175/1520-0426(2001)018<0376:HRDLFB>2.0.CO;2.

Iacono, M. J., J. S. Delamere, E. J. Mlawer, M. W. Shephard, S. A. Clough, and W. D. Collins, 2008: Radiative forcing by long-lived greenhouse gases: Calculations with the AER radiative transfer models. *J. Geophys. Res.*, **113**, D13103, doi:10.1029/2008JD009944.

Janjić, Z. I., 1994: The step-mountain eta coordinate model: Further developments of the convection, viscous sublayer, and turbulence closure schemes. *Mon. Wea. Rev.*, **122**, 927–945, doi:10.1175/1520-0493(1994)122<0927:TSMECM>2.0.CO;2.

——, 2001: Nonsingular implementation of the Mellor-Yamada level 2.5 scheme in the NCEP Meso model. NCEP Office Note 437, 61 pp. [Available online at http://www.emc.ncep.noaa.gov/officenotes/newernotes/on437.pdf.]

——, 2003: A nonhydrostatic model based on a new approach. *Meteor. Atmos. Phys.*, **82**, 271–285, doi:10.1007/s00703-001-0587-6.

——, 2005: A unified model approach from meso to global scales. *Geophysical Research Abstracts*, Vol. 7, Abstract 05582. [Available online at http://meetings.copernicus.org/www.cosis.net/abstracts/EGU05/05582/EGU05-J-05582.pdf.]

——, and T. L. Black, 2007: An ESMF unified model for a broad range of spatial and temporal scales. *Geophysical Research Abstracts*, Vol. 9, 05025. [Available online at http://meetings.copernicus.org/www.cosis.net/abstracts/EGU2007/05025/EGU2007-J-05025.pdf.]

——, and R. Gall, 2012: Scientific documentation of the NCEP Nonhydrostatic Multiscale Model on the B grid (NMMB). Part I Dynamics. NCAR Tech. Note NCAR/TN- 489+STR, 74 pp., doi:10.5065/D6WH2MZX.

Kalnay, E., 2003: *Atmospheric Modeling, Data Assimilation and Predictability*. Cambridge University Press, 341 pp.

Lorenc, A. C., 2003: The potential of the ensemble Kalman filter for NWP—A comparison with 4D-Var. *Quart. J. Roy. Meteor. Soc.*, **129**, 3183–3203, doi:10.1256/qj.02.132.

McKeen, S., and Coauthors, 2007: Evaluation of several PM$_{2.5}$ forecast models using data collected during the ICARTT/NEAQS 2004 field study. *J. Geophys. Res.*, **112**, D10S20, doi:10.1029/2006JD007608.

Mlawer, E. J., S. J. Taubman, P. D. Brown, M. J. Iacono, and S. A. Clough, 1997: Radiative transfer for inhomogeneous atmospheres: RRTM, a validated correlated-k model for the longwave. *J. Geophys. Res.*, **102**, 16 663–16 682, doi:10.1029/97JD00237.

Morss, R. E., and K. A. Emanuel, 2002: Influence of added observations on analysis and forecast errors: Results from idealized systems. *Quart. J. Roy. Meteor. Soc.*, **128**, 285–321, doi:10.1256/00359000260498897.

Musial, W., and B. Ram, 2010: Large-scale offshore wind power in the United States: Assessment of opportunities and barriers. National Renewable Energy Laboratory Tech. Rep. NREL/TP-500-40745, 221 pp. [Available online at http://www.nrel.gov/wind/pdfs/40745.pdf.]

Pichugina, Y., R. M. Banta, W. A. Brewer, S. P. Sandberg, and R. M. Hardesty, 2012: Doppler lidar–based wind-profile measurement system for offshore wind-energy and other marine boundary layer applications. *J. Appl. Meteor. Climatol.*, **51**, 327–349, doi:10.1175/JAMC-D-11-040.1.

Rogers, E., and Coauthors, 2009: The NCEP North American Mesoscale modeling system: Recent changes and future plans. Preprints, *23rd Conf. on Weather Analysis and Forecasting/19th Conf. on Numerical Weather Prediction*, Omaha, NE, Amer. Meteor. Soc., 2A.4. [Available online at http://ams.confex.com/ams/pdfpapers/154114.pdf.]

——, B. Ferrier, Z. Janjić, W. S. Wu, and G. DiMego, 2014: The NCEP North American Mesoscale (NAM) analysis and forecast system: Near-term plans and future evolution into a high-resolution ensemble. *Proc. 26th Conf. on Weather Analysis and Forecasting/22nd Conf. on Numerical Weather Prediction*, Atlanta, GA, Amer. Meteor. Soc., J1.3. [Available online at https://ams.confex.com/ams/94Annual/webprogram/Paper238898.html.]

Saha, S., and Coauthors, 2010: The NCEP Climate Forecast System Reanalysis. *Bull. Amer. Meteor. Soc.*, **91**, 1015–1057, doi:10.1175/2010BAMS3001.1.

Schwartz, M., D. Heimiller, S. Haymes, and W. Musial, 2010: Assessment of offshore wind energy resources for the United States. Tech. Rep. NREL/TP-500-45889, National Renewable Energy Laboratory, 96 pp. [Available online at http://www.nrel.gov/docs/fy10osti/45889.pdf.]

Semple, A., M. Thurlow, and S. Milton, 2012: Experimental determination of forecast sensitivity and the degradation of forecasts through the assimilation of good quality data. *Mon. Wea. Rev.*, **140**, 2253–2269, doi:10.1175/MWR-D-11-00273.1.

Skamarock, W. C., and Coauthors, 2008: A description of the Advanced Research WRF version 3. NCAR Tech. Note NCAR/TN-475+STR, 113 pp., doi:10.5065/D68S4MVH.

Smirnova, T. G., J. M. Brown, and S. G. Benjamin, 1997: Performance of different soil model configurations in simulating ground surface temperature and surface fluxes. *Mon. Wea. Rev.*, **125**, 1870–1884, doi:10.1175/1520-0493(1997)125<1870:PODSMC>2.0.CO;2.

——, ——, and ——, 2000: Validation of long-term precipitation and evolved soil moisture and temperature fields in MAPS. Preprints, *15th Conf. on Hydrology*, Long Beach, CA, Amer. Meteor. Soc., 43–46.

Strauch, R. G., D. A. Merritt, K. P. Moran, K. B. Earnshaw, and D. van de Kamp, 1984: The Colorado Wind Profiling Network. *J. Atmos. Oceanic Technol.*, **1**, 37–49, doi:10.1175/1520-0426(1984)001<0037:TCWPN>2.0.CO;2.

Thompson, G., P. R. Field, R. M. Rasmussen, and W. D. Hall, 2008: Explicit forecasts of winter precipitation using an improved bulk microphysics scheme. Part II: Implementation of a new snow parameterization. *Mon. Wea. Rev.*, **136**, 5095–5115, doi:10.1175/2008MWR2387.1.

Weber, B. L., D. B. Wuertz, D. C. Welsh, and R. McPeek, 1993: Quality controls for profiler measurements of winds and RASS temperatures. *J. Atmos. Oceanic Technol.*, **10**, 452–464, doi:10.1175/1520-0426(1993)010<0452:QCFPMO>2.0.CO;2.

White, A. B., and Coauthors, 2007: Comparing the impact of meteorological variability on surface ozone during the NEAQS (2002) and ICARTT (2004) field campaigns. *J. Geophys. Res.*, **112**, D10S14, doi:10.1029/2006JD007590.

Wilczak, J., E. E. Gossard, W. D. Neff, and W. L. Eberhard, 1996: Ground-based remote sensing of the atmospheric boundary layer: 25 years of progress. *Bound.-Layer Meteor.*, **78**, 321–349, doi:10.1007/BF00120940.

——, L. Bianco, J. Olson, I. Djalalova, J. Carley, S. Benjamin, and M. Marquis, 2014: The Wind Forecast Improvement Project (WFIP): A public/private partnership for improving short term wind energy forecasts and quantifying the benefits of utility operations. NOAA Final Tech. Rep. to DOE, Award DE-EE0003080, 159 pp. [Available online at http://energy.gov/sites/prod/files/2014/05/f15/wfipandnoaafinalreport.pdf.]

——, and Coauthors, 2015: The Wind Forecast Improvement Project (WFIP): A public–private partnership addressing wind energy forecast needs. *Bull. Amer. Meteor. Soc.*, **96**, 1699–1718, doi:10.1175/BAMS-D-14-00107.1.

Wolfe, D. E., and Coauthors, 2007: Shipboard multisensory merged wind profiles from the New England Air Quality Study 2004. *J. Geophys. Res.*, **112**, D10S15, doi:10.1029/2006JD007344.

Wu, W.-S., R. J. Purser, and D. F. Parrish, 2002: Three-dimensional variational analysis with spatially inhomogeneous covariances. *Mon. Wea. Rev.*, **130**, 2905–2916, doi:10.1175/1520-0493(2002)130<2905:TDVAWS>2.0.CO;2.